Pergamon

Prog. Aerospace Sci. Vol. 33, pp. 323–351, 1997

0376–0421/97 $32.00

PII: S0376–0421(96)00008-5

ENHANCED MIXING WITH STREAMWISE VORTICITY

I. A. Waitz,* Y. J. Qiu,† T. A. Manning,‡ A. K. S. Fung,* J. K. Elliot,* J. M. Kerwin,* J. K. Krasnodebski,* M. N. O'Sullivan,* D. E. Tew,* E. M. Greitzer,* F. E. Marble,§ C. S. Tan* and T. G. Tillman||

* *Gas Turbine Laboratory, Massachusetts Institute of Technology, Cambridge, MA 02139, U.S.A.;*
† *Aeroacoustics and Vibration Group, Carrier Corporation, Syracuse, NY, U.S.A.;*
‡ *Stanford University, Palo Alto, CA, U.S.A.;*
§ *California Institute of Technology, Pasadena, CA, U.S.A.;*
|| *United Technologies Research Center, East Hartford, CT, U.S.A.*

(*Received for publication* 2 *October* 1996)

Abstract—A quantitative description is presented of mixing augmentation mechanisms associated with embedded streamwise vortices. The specific context of interest is the flowfield downstream of convoluted (lobed) mixers, but the concepts developed apply to a range of devices that generate such vortices for enhanced mixing. Arguments are presented to illustrate the dependence of mixing augmentation on the strain field associated with the vortices; this strain field increases both the area available for mixing between two streams and the local gradients in fluid properties which provide the driving potential for mixing. Computations and experiments have been carried out to assess the influence of the streamwise vortices on both momentum interchange and mixing on a molecular level. Based on these investigations, scaling laws have been developed for the overall parametric trends of flow field structure and mixing rate as functions of lobe geometry, Reynolds number, stream-to-stream velocity ratio and Mach number. © 1997 Elsevier Science Ltd.

CONTENTS

1. INTRODUCTION AND SCOPE OF THE PAPER

There are a number of aerospace applications where methods to enhance fluid mixing between co-flowing streams have been identified as critical or enabling technologies. Examples include low-emissions combustors, ejectors for high lift or jet noise reduction, infrared suppressor nozzles, turbofan core-bypass mixers used to increase propulsive

efficiency and supersonic combustion ramjets. The requirements and the figures of merit for the mixing process depend on the application, as well as whether molecular mixing of chemical species, transfer of momentum, or transfer of energy is desired, but most criteria are related to the rapidity and spatial uniformity of the mixing process and the cost (frequently in terms of total pressure loss) associated with performing the mixing.

It is widely recognized that a powerful mechanism for enhancing mixing is the introduction of strong streamwise vortices. There are a variety of ways in which this idea has been implemented, but the basic concept of utilizing a streamwise vortical structure with its associated cross-stream circulation to augment the rate of mixing is fundamental to all of them.

The objectives of this paper are: (i) to describe the mechanisms responsible for *streamwise-vorticity-enhanced mixing*, and (ii) to quantify the mixing augmentation in several cases of practical interest. The approaches presented will be seen to apply to a range of devices that employ streamwise vorticity to enhance mixing, including lobed mixers for ejectors, wall-mounted vortex generators and many fuel injection schemes.

Two themes underlie the presentation of the material. The dominant one is the characterization of mixing processes based on the relative roles of flow structures associated with *streamwise* and *transverse* (such as in a planar shear layer) components of vorticity. Such decomposition is useful for providing insight into the three-dimensional mixing process and also as a basis for modeling the flow. A secondary theme is the utility of a slender-body approach for describing these three-dimensional flows, not only as a means for rapid computation but also, more importantly, to provide insight for modeling.

The paper begins with a description of the lobed mixing devices that were the focus of this study (Section 2), followed by a discussion of the morphology of incompressible mixing layers with large-scale, streamwise vortical structures (Section 3). The mechanisms responsible for mixing enhancement in these flows are then introduced and quantified (Section 4) for both laminar and turbulent flow regimes. Experimental and computational results are used to illustrate the mixing augmentation associated with the streamwise vortices downstream of a lobed mixer (Section 5). The description is then extended to compressible flow (Section 6), with characterization of the different physical effects due to operation at Mach numbers of unity or higher. The aim, throughout, is not so much to provide details of a specific configuration but rather insight into fluid mixing in a broad class of devices.

2. LOBED MIXERS AND STREAMWISE VORTICITY GENERATION

Lobed mixer geometries similar to that shown schematically in Fig. 1 were the basis for much of the work discussed in this paper. These geometries are well-suited to the study of mixing augmentation because they allow the controlled introduction of streamwise and transverse vorticity along the interface between co-flowing streams. They are also of considerable technological interest, for core-bypass mixing[1,2] and in ejectors for jet noise reduction.[20,23,24] Using lobed mixers, ejector pumping effectiveness has been measured to be 75% greater than with conventional geometries, providing evidence of the level of mixing augmentation associated with the streamwise vortices.[23] Impressively, these ejectors achieved 90–95% of the theoretical (complete mixing assumption) pumping value in a duct length equivalent to one duct diameter.

In a lobed mixer, the generation of streamwise vorticity is associated with the variation in aerodynamic loading along the *span* of the mixer, analogous to the situation along a finite wing. At the trailing edge, a continuous distribution of streamwise vorticity is discharged into the flow, evolving downstream into an array of discrete counter-rotating vortices, as shown in Fig. 1. The vortices grow through turbulent diffusion and the circulation eventually decays as the counter-rotating vortices diffuse into one another. The streamwise vortices downstream of such forced mixing devices are typically larger, in both magnitude and scale, than those in naturally developing free shear layers and boundary layers.

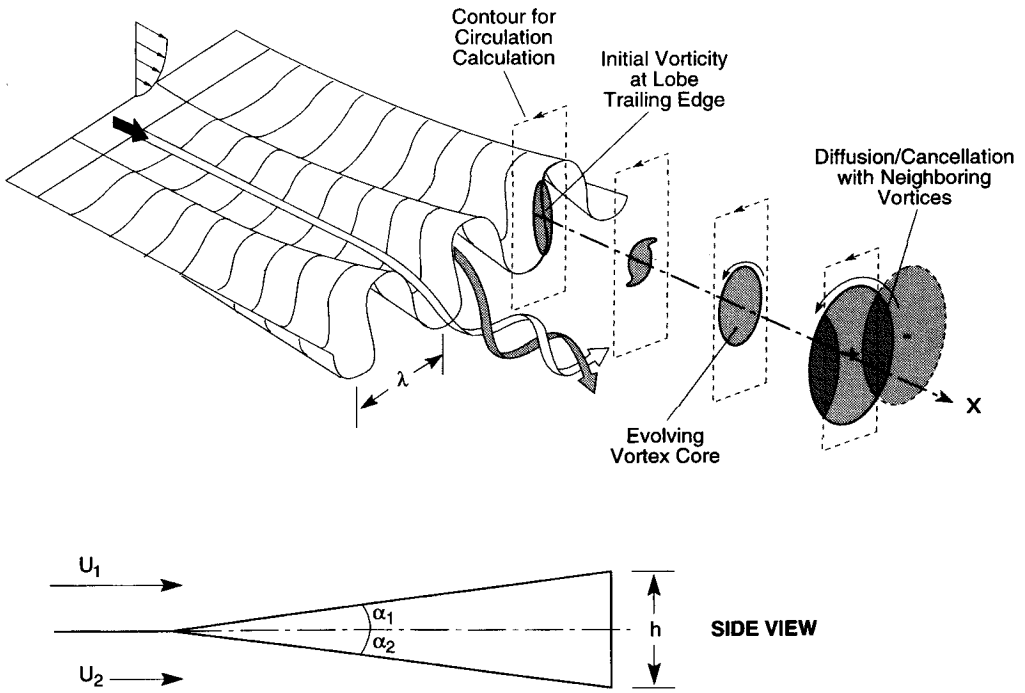

Fig. 1. Lobed mixer.

A good estimate for the initial streamwise circulation due to the lobes is given by assuming that the fluid which exits the lobes does so at the lobe angle.[24] For the geometry shown in Fig. 1 this yields a shed circulation, Γ_{te}, of magnitude

$$\Gamma_{te} \propto U_1 h \tan\alpha_1 + U_2 h \tan\alpha_2 \tag{1}$$

where U_1 and U_2 are the freestream velocities on either side of the lobe, h is the lobe height and α_1 and α_2 are the lobe penetration angles. For $\alpha_1 = \alpha_2 = \alpha$, Equation (1) reduces to

$$\Gamma_{te} \propto 2\bar{U} h \tan\alpha \tag{2a}$$

where $\bar{U}$ is the average freestream velocity, $(U_1 + U_2)/2$. A constant, C, whose value depends on the lobe geometry, is necessary in the scaling to provide a quantitative estimate of circulation. For mixers with vertical side walls, such as are examined in this study, the value of C can be taken as unity, i.e.

$$\Gamma_{te} = 2\bar{U} h \tan\alpha. \tag{2b}$$

Equation (2b) provides a useful and direct link between mixer geometry and shed circulation.

Skebe *et al.*[24] and O'Sullivan *et al.*[17] have characterized the range of geometries and flow conditions over which Equation (2b) applies. For lobes with half-angles, α, up to 22°, the circulation estimated from Equation (2b) is within 5% of values deduced from numerical simulations.[24] For larger angles, where the lobe boundary layers have a noticeable effect on the fluid exit angle, the concept can be extended by using an effective lobe penetration angle, α_{eff} and an effective lobe height, h_{eff}, to account for the boundary layer displacement thickness.

When the freestream velocities on either side of the lobe are not equal, as is most often the case in practical devices, vorticity components parallel to the trailing edge (transverse vorticity) are also present. An aspect of interest then is the interaction between transverse and streamwise vortical structures and the relative roles of the two types of structures in mixing.

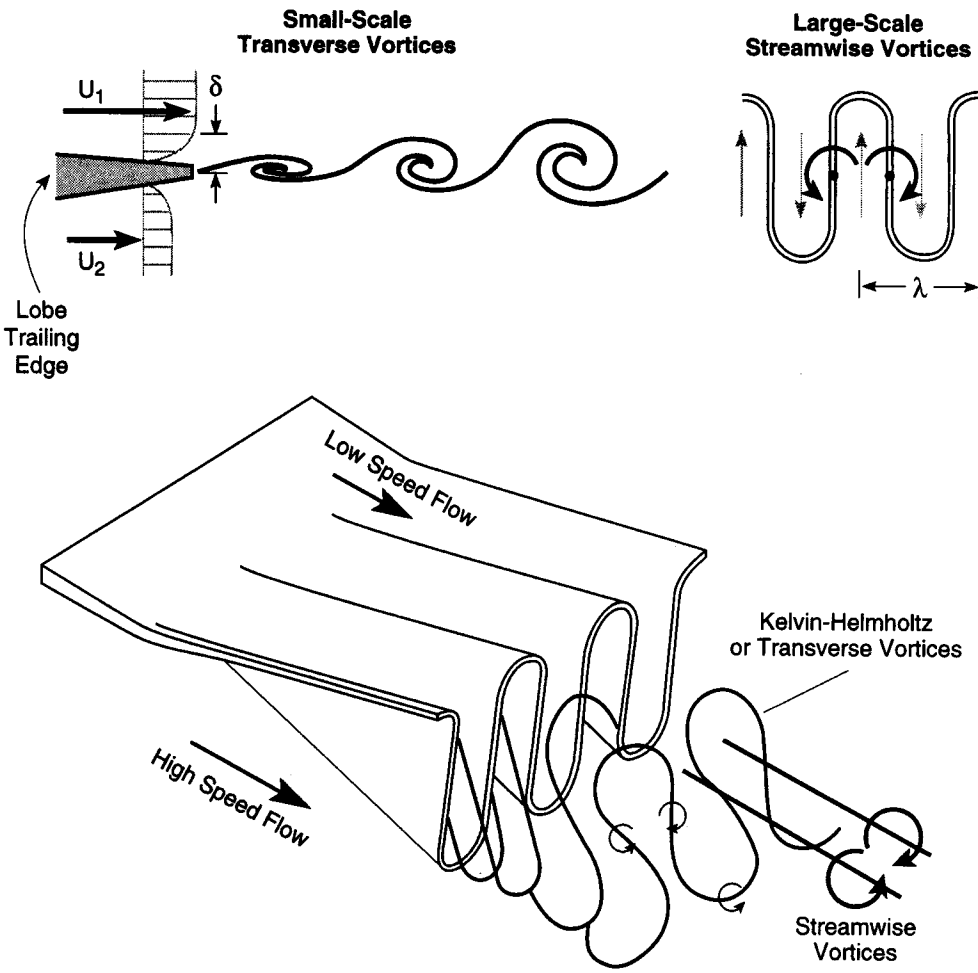

Fig. 2. Schematic of vortical structure about a lobed mixer (after McCormick[16]).

3. FLOW MORPHOLOGY AND RELEVANT LENGTH SCALES

A general description of the lobed mixer flow field can be separated conceptually into two parts: (i) the generation of the streamwise vorticity, which involves the fluid dynamics within the lobe; and (ii) the mechanisms and parametric dependence of mixing enhancement associated with the evolution of the flow downstream of the lobe. The latter are the focus of this article.

The important vortical elements in the downstream flow field are outlined schematically in Fig. 2. The counter-rotating pairs of streamwise vortices are the largest scale structures in the flow for three to ten lobe wavelengths downstream. There are also transverse vortices associated with the instability of the shear layer between the two streams of different velocity on either side of the plate.[12,16,21] Horseshoe vortices can also be formed around the front of the lobes; in typical geometries these have circulation an order of magnitude less than either transverse or streamwise vortices and have little impact on the overall mixing process.[16] Flow visualization photographs of this region are presented in Fig. 3.[12] The photographs were obtained using a gravity-driven water tunnel with two independently controlled streams*. Photographs of two conditions are shown, one with Reynolds number,

* The data were obtained using phenolphthalein seeded in one stream, and sodium hydroxide in the other. The two streams are initially clear, but when mixing at the molecular level has brought the local pH to a level between 8 and 12, the product turns a vivid red.[4]

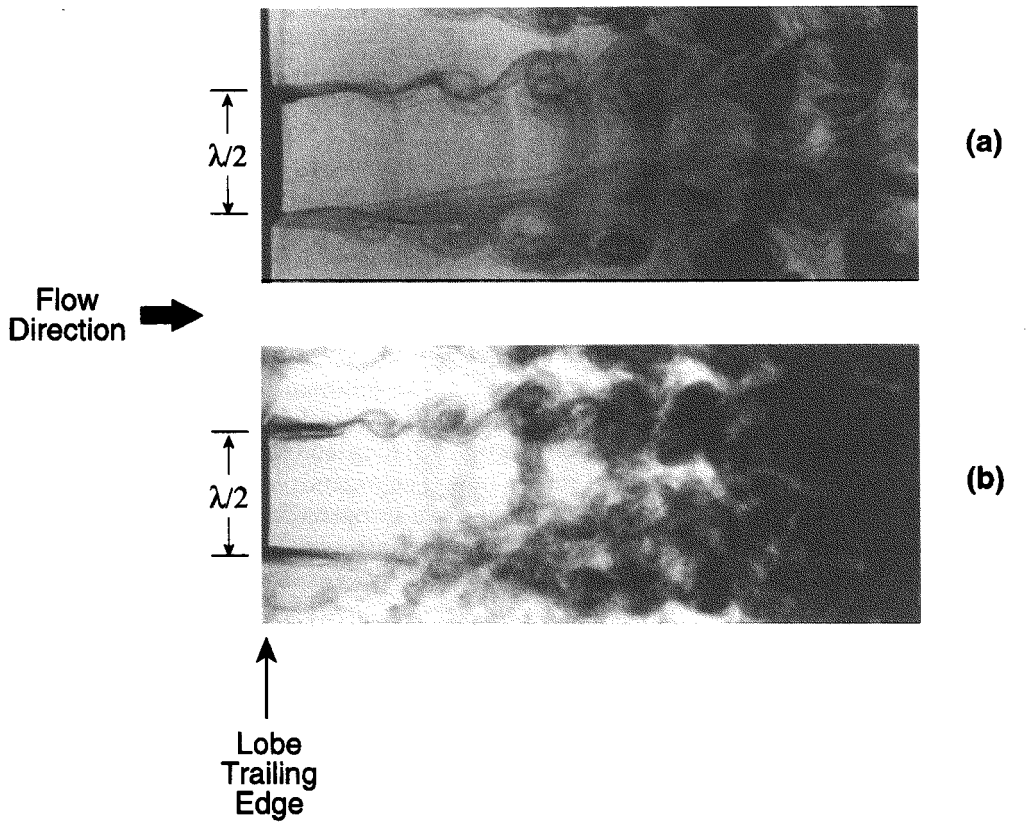

Fig. 3. Production of small scale structure downstream of forced mixer: velocity ratio $s = 0.5$: (a) $Re = 900$; (b) $Re = 3600$.[12]

Re, (based on mean velocity and lobe wavelength) of 900 and the second with $Re = 3600$. The view is from above looking down upon the row of lobes, with the flow from left to right. In both cases, the ratio of the freestream velocities was, $s = U_1/U_2 = 0.5$. The transverse vortex structures can be seen in both pictures, but in the higher Reynolds number flow, transition to turbulent mixing has occurred.

There is an important difference in length scale between the motions associated with streamwise and transverse vorticity. The scale of the former is set by the vortex spacing, in other words the half-wavelength of the lobe geometry, $\lambda/2$. The initial scale of the latter is set by the shear layer thickness at the trailing edge, similar to the situation in planar shear layers. For lobed mixers, the boundary layer on the lobe peaks and vertical edges may be thinned by more than a factor of five when compared to the boundary layer upstream of the lobes. For geometries of technological interest, then the scale of the transverse vortical motions is thus small compared to that of the streamwise vortices for a distance downstream of approximately three to ten wavelengths when, depending on geometry, the transverse layer will have diffused to a length comparable with $\lambda/2$. For example, in a turbofan mixer $Re = 0(10^6$–$10^7)$, lobe spacing is approximately 0.2 m and the boundary layer thickness at the trailing edge is less than 0.02 m.

The difference in scale between streamwise and transverse vortices allows adoption of a simplified view of the principal mechanisms for interaction between the two structures. In this view, transverse vorticity is associated with turbulent transport which diffuses streamwise vorticity across the symmetry planes between the counter-rotating streamwise vortices, thereby reducing the magnitude of the streamwise circulation. The streamwise vortices produce stretching along the axes of the transverse vortices. In the present treatment, we compute the dynamical effects due to the streamwise vortices, while modeling the smaller scale dynamics associated with the transverse vorticity.

4. VORTEX-ENHANCED MIXING

We now turn to the mechanisms responsible for mixing enhancement in these flows. When an interface between two fluids of different properties (e.g. chemical composition, momentum or energy) is convected in the velocity field of a vortex, the stretching of the interface creates two interrelated effects. The first is an increase in interfacial surface area and the second is an increase in the magnitude of gradients normal to the interface, both effects augment mixing.

The key elements of this process can be introduced by considering the model problem of a laminar diffusion flame in the field of an isolated vortex. The discussion presented below follows that given by Marble[13, 14] and Karagozian and Marble[10] for the two-dimensional case. The process elements are presented in steps. The effect of strain on rate of reaction for a planar diffusion flame is reviewed first (Section 4.1), followed by an assessment of the influence on mixing of the strain field associated with a two-dimensional vortex (Section 4.2). A slender-body approach is then used (Section 4.3) to extend Marble's two-dimensional unsteady results to three-dimensional steady flow. The analysis leads to relationships for predicting mixing augmentation in both laminar and turbulent flows. These relationships are evaluated using results of computations and experiments in Section 5.

4.1. EFFECT OF STRAIN ON MIXING

To illustrate the effect of strain on mixing, we consider two semi-infinite regions separated by the x-axis, one region containing fuel and the other oxidizer, as shown in Fig. 4a. The chemical kinetics are taken to be infinitely fast so that locally the reaction is diffusion controlled and the stoichiometry is taken such that equal amounts of oxidizer and fuel are consumed by the reaction in an infinitely thin reaction zone. Effects of heat release are neglected.

4.1.1. *No Strain: Mixing due to Pure Diffusion*

With no strain, the mixing process is pure diffusion described by

$$\frac{\partial K}{\partial t} = D\frac{\partial^2 K}{\partial y^2} \tag{3}$$

where K is the concentration of either reactant and the constant D is the binary diffusion coefficient. The solutions for the fuel and oxidizer concentrations, K_f and K_o,

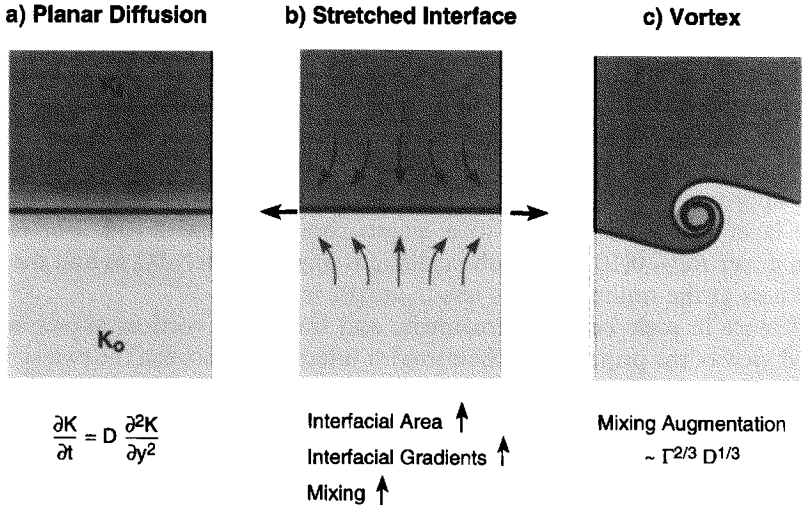

Fig. 4. Effect of strain on mixing at an interface.

respectively, are[14]

$$K_f = \text{erf}(y/\sqrt{4Dt}) \quad \text{and} \quad K_o = -\text{erf}(y/\sqrt{4Dt}) \tag{4}$$

where y is the coordinate normal to the interface and erf is the error function. Equation (4) shows that the thickness of the diffusion zone grows as $(Dt)^{1/2}$. The reactant consumption rate, which is a direct measure of the molecular mixing, may be expressed as the mass flux of either species at the reaction zone;

$$\rho D \frac{\partial K}{\partial y}\bigg|_{y=0} = \rho \left[\frac{D}{\pi t}\right]^{1/2}. \tag{5}$$

For pure diffusion, the rate of mixing approaches zero as $t \to \infty$.

4.1.2. *Mixing Augmentation due to Normal Strain*

Suppose a normal strain rate,* $\varepsilon = \partial u_x/\partial x = -\partial u_y/\partial y$, is applied to the flow field as shown schematically in Fig. 4b. A velocity normal to the interface now exists, $u_y = -\varepsilon y$, so the mixing process is described by

$$\frac{\partial K}{\partial t} - \varepsilon(t) y \frac{\partial K}{\partial y} = D \frac{\partial^2 K}{\partial y^2}. \tag{6}$$

Equation (6) can be transformed into the form of eqn (3) with the substitution

$$\zeta = y \exp\left[\int_0^t \varepsilon \, dt\right], \quad \tau = \int_0^t \left[\exp\left(\int_0^{t_2} 2\varepsilon \, dt_1\right)\right] dt_2 \tag{7}$$

and the solutions for the reactant concentrations are:

$$K_f = \text{erf}\,(\zeta/\sqrt{4D\tau}) \quad \text{and} \quad K_o = -\text{erf}(\zeta/\sqrt{4D\tau}). \tag{8}$$

The modification of the mixing behavior due to strain can be seen most readily for the case of constant strain rate, ε. In this case differentiation of Equation (8) gives the reactant consumption rate as:

$$\rho D \frac{\partial K}{\partial y}\bigg|_{y=0} = \rho \sqrt{\frac{2\varepsilon D}{\pi}} \left[\frac{e^{2\varepsilon t}}{e^{2\varepsilon t}} - 1\right]^{1/2}.$$

For small times or small strain rate, $t \ll 1/\varepsilon$, the reactant consumption rate is similar to the unstrained case. For large strain rate or long times, $t \gg 1/\varepsilon$, however, the consumption rate does not go to zero, but approaches the constant value $(2D\varepsilon/\pi)^{1/2}$. Strain enhances the reaction rate by increasing the interfacial surface area and increasing gradients in the diffusion zone. Mixing augmentation in a vortex flow field is due to the same physical effects, but in a geometrically more complex situation.

4.2. MIXING AUGMENTATION DUE TO A TWO-DIMENSIONAL VORTEX

The velocity field of a two-dimensional vortex located on the interface between the reactants in a constant density flow has only one non-zero component, u_θ, which is described by

$$\frac{\partial u_\theta}{\partial t} = \nu \frac{\partial}{\partial r}\left[\frac{1}{r}\frac{\partial}{\partial r}(r u_\theta)\right] \tag{9}$$

* Shearing does not affect the flow since there is no dependence on x.

Equation (9) is satisfied by[3]

$$u_\theta = (\Gamma/2\pi r)\left\{1 - \exp\left[\frac{-r^2}{4\nu t}\right]\right\}. \tag{10}$$

Equation (10) represents a vortex of circulation Γ with a viscous core that grows over time.

If the reaction and the vortex are both initiated at time $t = 0$, with increasing time the interface is stretched into a spiral, as shown in Fig. 4c. In the portion of the flow undergoing solid body rotation, however, the interface is not stretched, so the increase in interfacial length can be computed by examining only the region outside the viscous core. For a material element of initial length dl_o, the deformed length, dl, behaves as[14]

$$dl = \left[1 + \left(\frac{\Gamma t}{\pi r^2}\right)^2\right]^{1/2} dl_o \tag{11}$$

or, for large values of $\Gamma t/\pi r^2$,

$$dl = \frac{\Gamma t}{\pi r^2}\, dl_o. \tag{12}$$

Equation (12) shows that the local interfacial length increases roughly linearly in time for large values of $\Gamma t/\pi r^2$. Further, because the stretching takes place in the region outside of the viscous core of the vortex, this behavior is roughly independent of the growth rate of the core and thus the scaling applies to turbulent as well as laminar vortex flows. This stretching of the interface is the principal agent for mixing augmentation.

As with the planar diffusion flame, the reactant consumption rate gives a direct measure of mixing. For the velocity field of Equation (10), Marble[14] has shown that the augmentation in fuel consumption rate $\mathscr{M}_a$, (fuel consumption rate minus fuel consumption rate with no vortex) scales with $\Gamma^{2/3}D^{1/3}$:

$$\frac{\mathscr{M}_a}{\Gamma^{2/3}D^{1/3}} \cong 2\left(\frac{3}{2\pi}\right)^{2/3} + O\left(\frac{D}{\Gamma}\right)^{1/6} \tag{13}$$

and

$$A_{\text{mixed}} \cong 2\left(\frac{2}{2\pi^2}\right)^{1/3} \Gamma^{2/3} D^{1/3} t + O\left(\frac{D}{\Gamma}\right)^{1/2} \tag{14}$$

where A_{mixed} is the cross-sectional area of the fully mixed core.* The form of the expression for core area (Equation (14)) can be directly compared with that for pure radial diffusion, in which the core area grows at a rate proportional to Dt. The rate shown above is greater by a factor of $(\Gamma/D)^{2/3}$. Equation (13) provides a useful scaling for mixing augmentation as a function of diffusion coefficient (D) and vortex strength (Γ). The analysis is valid for any diffusion process (e.g. heat transfer) which may be written in the form of Equation (3).

4.3. MIXING AUGMENTATION DUE TO A THREE-DIMENSIONAL VORTEX: SLENDER-BODY APPROACH

The results of Section 4.2 for two-dimensional, unsteady flow can be extended to steady, three-dimensional vortices using a slender-body approximation, as introduced by Marble *et al.*[15] in studies of shock-enhanced mixing. The approach is illustrated conceptually for a lobed mixer in Fig. 5.[21] The three-dimensional spatial development downstream of the mixer is represented by the evolution of a two-dimensional unsteady flow field. Changes along the x-direction are viewed as changes with time seen by an observer traveling with an appropriate convection velocity, taken here as the mean through flow velocity, $\bar{U}$. Time is thus related to streamwise distance by $t = x/\bar{U}$. The ability to characterize an appropriate

*The results are for $R_\Gamma(Sc)^{-1/2} > 300$ where $R_\Gamma = \Gamma/\nu$ is the Reynolds number based on circulation and Sc is the Schmidt number, ν/D. For $R_\Gamma(Sc)^{-1/2} \lesssim 300$, the viscous core grows at a rate which is significant compared to the rate at which the burned-out core radius grows and the results are different.[14]

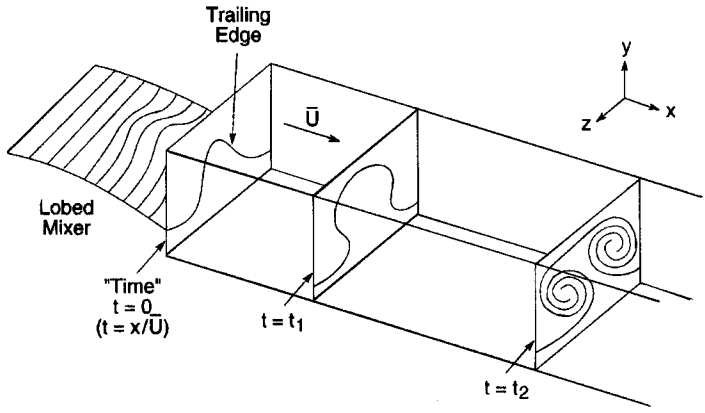

Fig. 5. Slender-body analogy for lobed mixer flow field development.[21]

convection velocity, as well as the difference in scale of the transverse and streamwise vortices, enable this modeling approach.

The conditions under which the slender body approach is justified are developed below. To assess the degree to which these conditions are met in devices of practical interest, a detailed comparison has been made between slender body analyses and fully three-dimensional Reynolds-averaged, Navier–Stokes computations of mixer nozzle flow fields. Appendix A describes the results of the comparisons, but, in sum, they show that the slender body analysis provides a useful and effective method for investigating parametric dependencies of mixing strategies, with computational times one to two orders of magnitude shorter than for three-dimensional solutions.

For a three-dimensional, steady, incompressible flow, we express the axial velocity, u, as the sum of the mean velocity and a (steady) perturbation to the mean; $u = \bar{U} + u'$, where $|u'/\bar{U}| \ll 1$. Since the dynamics of the cross-plane flow are dominated by the streamwise vortex, the cross-flow velocities are expected to scale with Γ/λ and cross flow lengths are expected to scale with λ, where Γ is the shed streamwise circulation and λ is the cross stream length scale characterizing the streamwise vortex.Thus the non-dimensional velocities and distances are

$$u_y^* = \frac{u_y \lambda}{\Gamma}, \quad u_z^* = \frac{u_z \lambda}{\Gamma}, \quad y^* = \frac{y}{\lambda} \quad \text{and} \quad z^* = \frac{z}{\lambda}.$$

With this scaling, time is non-dimensionalized by Γ/λ^2, so the relationship between non-dimensional time in the slender-body system and axial distance (x) in the three-dimensional system is given by

$$t^* = \frac{\Gamma x}{\bar{U}\lambda^2}. \tag{15}$$

The expression for t^* implies that two flows of different properties appear similar at axial distances corresponding to the same t^*.

The slender-body approximation is based on cross-plane velocities being small compared to the mean axial velocity, so that,

$$\frac{\Gamma}{\bar{U}\lambda} \ll 1. \tag{16}$$

If we assume that cross flow pressure gradients are much stronger than axial pressure gradients, the axial momentum equation becomes decoupled from the cross flow

momentum equations. If so, neglecting terms of $O(\Gamma/\bar{U}\lambda)^2$ yields the resulting system of equations:

$$\frac{\partial u_y^*}{\partial t^*} + u_y^* \frac{\partial u_y^*}{\partial y^*} + u_z^* \frac{\partial u_y^*}{\partial z^*} = -\frac{\partial p}{\partial y^*} + \frac{1}{R_\Gamma}\left(\frac{\partial^2}{\partial y^{*2}} + \frac{\partial^2}{\partial z^{*2}}\right) u_y^* \tag{17}$$

$$\frac{\partial u_z^*}{\partial t^*} + u_y^* \frac{\partial u_z^*}{\partial y^*} + u_z^* \frac{\partial u_z^*}{\partial z^*} = -\frac{\partial p}{\partial z^*} + \frac{1}{R_\Gamma}\left(\frac{\partial^2}{\partial y^{*2}} + \frac{\partial^2}{\partial z^{*2}}\right) u_z^* \tag{18}$$

$$\frac{\partial u_y^*}{\partial y^*} + \frac{\partial u_z^*}{\partial z^*} = 0 \tag{19}$$

where $R_\Gamma = \Gamma/\nu$ is the circulation Reynolds number. These equations are written for laminar flow, with viscosity ν, but can be extended to turbulent flow as will be shown below. The diffusion of a scalar quantity ϕ can also be described in slender-body form

$$\frac{\partial \phi}{\partial t^*} + u_y^* \frac{\partial \phi}{\partial y^*} + u_z^* \frac{\partial \phi}{\partial z^*} = \frac{D}{\Gamma}\left(\frac{\partial^2}{\partial y^{*2}} + \frac{\partial^2}{\partial z^{*2}}\right) \phi. \tag{20}$$

These approximations allow extension of the Marble[14] scaling (Section 4.2) to three-dimensional streamwise vortices. The augmentation in mixing rate expressed in Equation (13) can be written for the analogous three-dimensional flow as

$$\frac{\partial \mathscr{M}_a}{\partial t^*} \propto \left(\frac{D}{\Gamma}\right)^{1/3} \tag{21}$$

or equivalently

$$\frac{\partial \mathscr{M}_a}{\partial (x/\lambda)} \propto \frac{\Gamma^{2/3} D^{1/3}}{\bar{U}\lambda}. \tag{22}$$

In Equations (19) and (20) $\mathscr{M}_a$ represents the augmentation in mixing (or reactant consumption) due to the introduction of the streamwise vortex, i.e. that portion of the mixing above and beyond that which would occur purely due to diffusion on a planar interface. Equation (22) provides a direct scaling for the axial mixing augmentation rate as a function of Γ, $\bar{U}$, λ and D.

4.4. EXTENSION TO TURBULENT FLOW

The scaling described can be extended to turbulent flow by employing a turbulent 'effective diffusivity', D_t, to characterize the small scale mixing due to the transverse turbulent motion. The principal assumption is that mixing on this scale is independent of curvature and strain associated with the streamwise vortex. Although this cannot be true for all flow regimes, the success of the scaling based on this approximation for lobed mixers implies that the assumption is justified for the parameter ranges investigated.

As a starting point, we again make use of the slender body approach and consider an unsteady, two-dimensional flow field associated with a turbulent vortex. The velocity field of the vortex, as well as the diffusion process, are different from laminar flow. The velocity field must satisfy the momentum equation

$$\frac{\partial u_\theta}{\partial t} = \nu_t(t) \frac{\partial}{\partial r}\left[\frac{1}{r}\frac{\partial}{\partial r}(r u_\theta)\right] \tag{23}$$

where the turbulent viscosity, ν_t, will in general vary with time (i.e. distance downstream if a slender body approach is adopted). Equation (6) for diffusion on an interface is also modified

$$\frac{\partial K}{\partial t} - \varepsilon(t) y \frac{\partial K}{\partial y} = D_t(t) \frac{\partial^2 K}{\partial y^2}. \tag{24}$$

To proceed further, we need to specify the functional dependence of ν_t and D_t on time. Since time is directly proportional to length in the slender body analysis, we can make use of the

extensive planar shear layer measurements that show that turbulent viscosity (and diffusivity) vary linearly with downstream distance.[5, 7] Specifically, the measurements show that the behavior of the shear layer vorticity thickness*, δ_v, is given by

$$\frac{\delta_v}{x} \propto \frac{1-r}{1+r} \tag{25}$$

where r is the velocity ratio, U_1/U_2. Then, as described in a number of texts,[22] a scaling for the diffusivity based on shear layer thickness may be derived based on Prandtl's mixing length hypothesis such that

$$\nu_t = Sc_t/D_t \approx \delta_v(x)\,\Delta U = B\left(\frac{1-r}{1+r}\right)^2 \bar{U}x \tag{26}$$

where B is an empirical constant and Sc_t is the turbulent Schmidt number.

Neglecting spatial variation of the turbulence properties in the cross plane, the turbulent viscosity thus varies linearly with convective time such that $\nu_t = \beta t$, where

$$\beta = B\left(\frac{1-r}{1+r}\right)^2 \bar{U}^2. \tag{27}$$

Substituting into Equation (23) and solving for u_θ, we find

$$u_\theta = (\Gamma/2\pi r)\left\{1 - \exp\left[\frac{-r^2}{4\beta t^2}\right]\right\}. \tag{28}$$

The equation describing diffusion about a strained interface with turbulent mixing (Equation (24)) has a similarity solution, similar to that for laminar mixing (Equation (8)) given by

$$K = \pm \operatorname{erf}\left(\frac{ye^{\varepsilon t}}{2\left[\left(\frac{\beta}{Sc_t}\right)\int_0^t t_1 e^2 \int_0^{t_1} \varepsilon(t_2)\,dt_2 dt_1\right]^{1/2}}\right) \tag{29}$$

where again, $\varepsilon = \varepsilon(t)$. Equations (28) and (29) can be used to extend the Marble vortex/diffusion flame analysis to turbulent flow. The mathematics are somewhat complicated but the leading term describing the mixing augmentation is similar to that of Equation (13), however the laminar diffusion coefficient is replaced by the turbulent version, D_t, described above. The result is[9]

$$\frac{\text{Augmentation in consumption rate}}{\Gamma^{2/3} D_t^{1/3}} = \left(\frac{4\sqrt{2}}{\pi}\right)^{2/3} + O\left(\frac{D_t}{\Gamma}\right)^{1/6}. \tag{30}$$

For turbulent flow downstream of a lobed mixer therefore, mixing augmentation due to streamwise vortices would be expected to scale as

$$\left(\frac{d\mathcal{M}_a}{dt^*}\right) \propto \left(\frac{D_t}{\Gamma}\right)^{1/3} \tag{31a}$$

or

$$\left(\frac{\partial \mathcal{M}_a}{\partial(x/\lambda)}\right) \propto \frac{\Gamma^{2/3} D_t^{1/3}}{\bar{U}\lambda}. \tag{31b}$$

Thus the scaling is essentially unchanged whether a laminar or turbulent mixing process is assumed.

When applied to a lobed mixer flow, turbulent diffusion may be expressed as a function of the velocities on either side of the lobe (Equation (26)), with circulation related to the

* Here vorticity thickness is defined as the difference between the velocities of the high and low speed streams divided by the magnitude of the maximum velocity gradient, $\delta_v = (U_2 - U_1)/|du/dy|_{max}$.

lobe geometry by Equation (1). This scaling can therefore be used to estimate mixing augmentation due to streamwise vortices for different lobe geometries and flow conditions. In Section 5, we will use experiments and computations to examine over what parameter ranges this scaling applies.

5. MIXING ENHANCEMENT IN LOBED MIXER FLOWS

5.1. EFFECT OF STREAMWISE VORTICITY ON INTERFACE LENGTH

Using the ideas developed concerning mixing enhancement, we can now examine specific questions relating to mixer lobe flow behavior. There are two effects that enhance mixing compared to naturally developing shear layers. One is the increase in initial interfacial area (interface length), compared to a flat splitter, provided by convoluting the trailing edge. The second effect is the further increase in interfacial area and steepening of interfacial gradients downstream from the trailing edge due to cross-stream convection associated with streamwise vorticity. Both of these effects are apparent in the slender body simulation of the flow downstream of a lobed mixer shown in Fig. 6. The mixing of a scalar, initially specified at $\phi = -1$ on one side of the lobe and $\phi = +1$ on the other, is shown at different distances (times) downstream from the mixer lobe. The results were obtained using a spectral element Navier–Stokes code which is described in Appendix A.

For lobed mixers with nearly rectangular trailing edge profiles, the initial interface length is given by

$$\frac{l}{\lambda} \approx 2\left(\frac{h}{\lambda}\right) + 1. \tag{32}$$

For typical lobed mixers ($h/\lambda = 1$ to 3) this effect increases the initial mixing rate by a factor of 3–7. The increase in interfacial area downstream from the lobe trailing edge can be found by integrating the expression for dl (Equation (12)) over the trailing edge of the lobe. The inner bound for the integration is the radius of the viscous vortex core which is assumed to

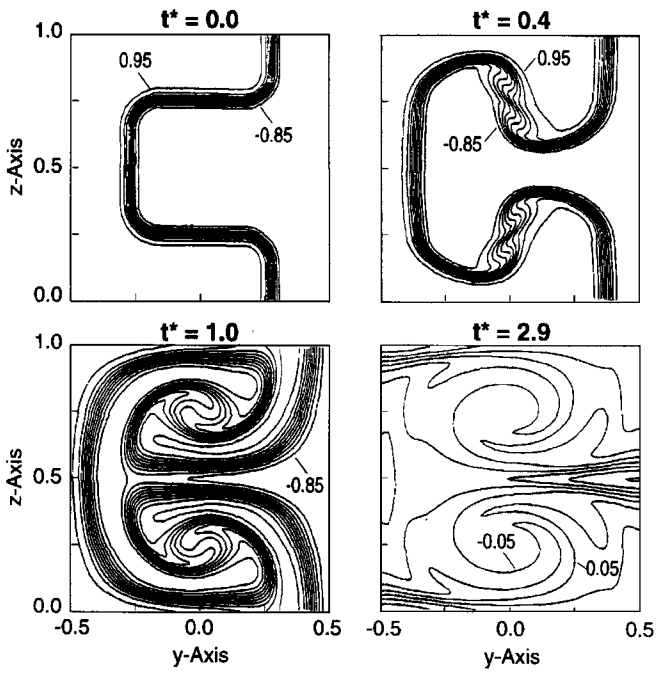

Fig. 6. Transport of scalar in a lobed mixer flow.[21]

be some constant fraction of the lobe spacing (e.g. $\lambda/4$). The increase in interfacial surface area is found to be approximately linear with downstream distance from the trailing edge and proportional to the strength of the shed circulation,

$$\frac{d(l/\lambda)}{d(x/\lambda)} \approx C \frac{\Gamma}{\bar{U}\lambda} \tag{33a}$$

or

$$\frac{d(l/\lambda)}{dt^*} \approx C \tag{33b}$$

where C is a function of lobe geometry. This linear behavior is evident in the steady, three-dimensional Euler simulations shown in Fig. 7[8] where the mean interface length is plotted as a function of downstream distance for two different lobed mixers. The growth in mean interface length due to the streamwise vortex can be rapid, with the interface tripling in length in the first two wavelengths downstream of the trailing edge. The ratio of the computed non-dimensional circulations for the two geometries shown in Fig. 7 is 6.0 and the ratio of the interface length growth rates is 6.5, in close agreement with the scaling based on non-dimensional circulation suggested by Equation (33a). Tew[26] has performed additional steady and unsteady Euler computations for several different lobe geometries and velocity ratios and found that for inviscid flows the constant in Equation (33) is approximately $C \approx 1.3$.

Linear interface growth is also seen in the results of three-dimensional Navier–Stokes simulations reported by Krasnodebski,[11] but the interface growth rate is slower with $C \approx 0.4$–0.5 because of the presence of turbulent diffusion which tends to cause more rapid decay of circulation and also because of the finite vortex sheet thickness associated with the boundary layers shed from the lobe. The growth rate shown in the viscous solutions has the interface length doubling in two to three wavelengths and this situation is more representative of practical situations. For typical mixer applications, where $h/\lambda \approx 1$–3, mixing enhancement due to initial interface length and to vortex augmentation are of roughly the same size. We will quantify these effects more rigorously below using results of computations and experiments.

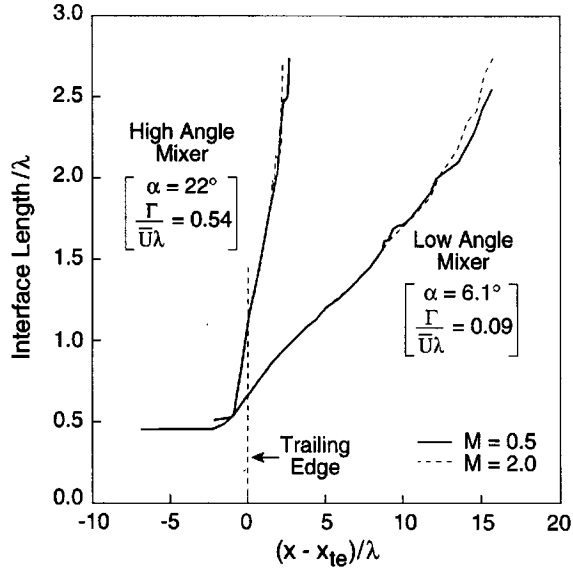

Fig. 7. Axial evolution of interface length (Euler calculation, $t = 1.0$).[8]

5.2. COMPUTATIONAL ASSESSMENT

5.2.1. *Laminar Flow*

The effect of the increased initial trailing edge length of the lobed mixer can be separated from the effect due to the streamwise vortices by comparing the results of two slender-body Navier–Stokes computations: (1) a simulation of a lobed mixer flow field; and (2) a computation of the diffusion of a scalar for the same trailing edge geometry with no streamwise vorticity (a convoluted plate). An example is shown in Fig. 8, for laminar flow, where scalar mixedness for the two different cases is plotted as a function of non-dimensional time. Here the scalar mixedness parameter, $\mathcal{M}$, is defined as

$$\mathcal{M} = \frac{1}{A}\int_A (1 - |\phi|)\, dA \tag{34}$$

where A is the mixing duct cross-sectional area. The scalar mixedness can be interpreted directly as the amount of product in a diffusion-limited, bi-molecular reaction with equivalence ratio of unity (the basis for the diffusion flame models discussed in Sections 4.1 and 4.2). The difference between the curves shown in Fig. 8 is the augmentation due to the streamwise vortex, $\mathcal{M}_a$, which is expected to scale as

$$\left(\frac{d\mathcal{M}_a}{dt^*}\right) \propto \left(\frac{D}{\Gamma}\right)^{1/3} \propto ((R_\Gamma Sc)^{-1/3}) \tag{35}$$

based on Equation (21).

The scaling can be tested by examining different circulation Reynolds numbers, $R_\Gamma = \Gamma/\nu$, as in Fig. 9, which shows the scalar field at $t^* = 0.4$ for two cases with the same initial conditions, but with Reynolds numbers differing by a factor of four. The thinning of the concentration boundary layer for the higher Reynolds number case is apparent. The mixing augmentation for these two cases is plotted as a function of non-dimensional time in Fig. 10. Also shown is the result obtained when the higher Reynolds number case is scaled by the ratio of the diffusion coefficients ($D \propto \nu$) to the one-third power as suggested by Equation (35). There is agreement in slope between the two cases for $1 \lesssim t^* \lesssim 2$ where the mixing rate is constant, as suggested by the vortex diffusion flame models described in Section 4.3. The departure of the two curves farther downstream arises because of differences between the velocity field of a confined array of counter-rotating vortices and that of a single vortex, for which the scaling law was derived. For the counter-rotating vortex array, diffusion between vortices of opposite sign causes a marked decay in streamwise circulation.

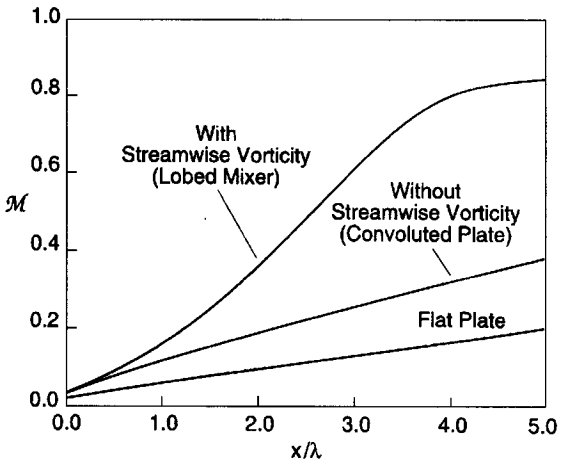

Fig. 8. Comparison of mixedness as a function of downstream distance (x/λ) for flows with streamwise vorticity and without streamwise vorticity (convoluted plate and flat plate). $Re = 2000$, $\Gamma/\bar{u}\lambda = 0.39$ and $Sc = 1.0$.[21]

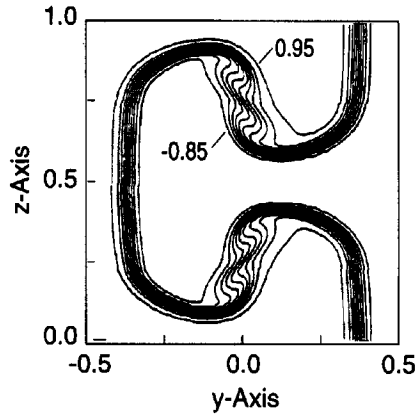

(a) $Re_\Gamma = 1000$

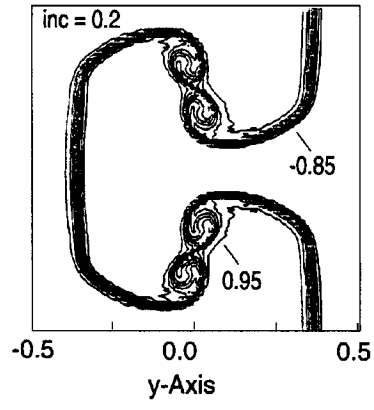

(b) $Re_\Gamma = 4000$

Fig. 9(a) and (b). Contours of scalar value at $t^* = 0.4$, $h/\lambda = 0.54$ and $Sc = 1.0$.[21]

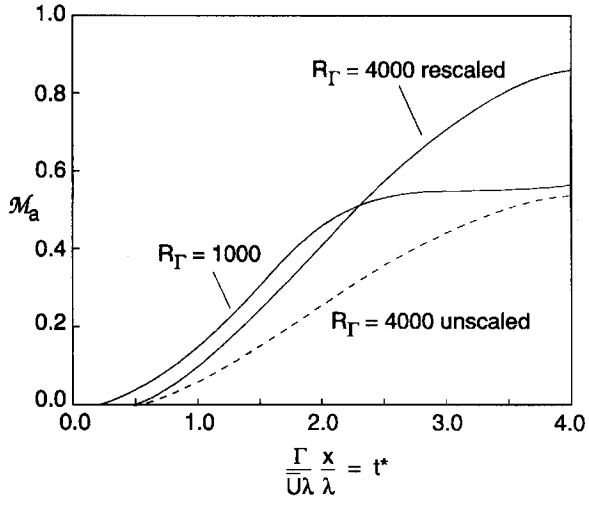

Fig. 10. Mixing augmentation for $R_\Gamma = 1000$ and $R_\Gamma = 4000$, rescaled in accordance with the vortex diffusion flame model; $h/\lambda = 0.54$, $Sc = 1.0$.[21]

The scaling laws have been examined over a broader range of Reynolds numbers and lobe shapes, using the slender-body code. The results are shown in Fig. 11 which presents the maximum mixing augmentation rate as a function of circulation Reynolds number for two different values of h/λ. The mixing behavior can be roughly divided into two regimes separated by a critical circulation Reynolds number, $R_{\Gamma crit}$. For circulation Reynolds numbers greater than $R_{\Gamma crit}$, the flows are characterized by vorticity which has coalesced into well-defined streamwise vortices, with the maximum mixing rate proportional to $(R_\Gamma)^{-1/3}$, consistent with the Marble vortex/diffusion flame model. For circulation Reynolds numbers less than $R_{\Gamma crit}$, there is appreciable diffusion of vorticity between the counter-rotating vortices prior to formation of a vortex core and the vortex scaling law does not apply. For example, for $h/\lambda = 0.54$ and $R_\Gamma = 100$, the streamwise circulation is less than 50% of its initial value by $t^* = 2$.

5.2.2. *Turbulent Flow*

The results presented in Figs 10 and 11 were for laminar flow (constant diffusion coefficient). Computations have also been carried out for a diffusion coefficient which varies linearly in time to simulate the turbulent diffusion driven by a difference in velocity

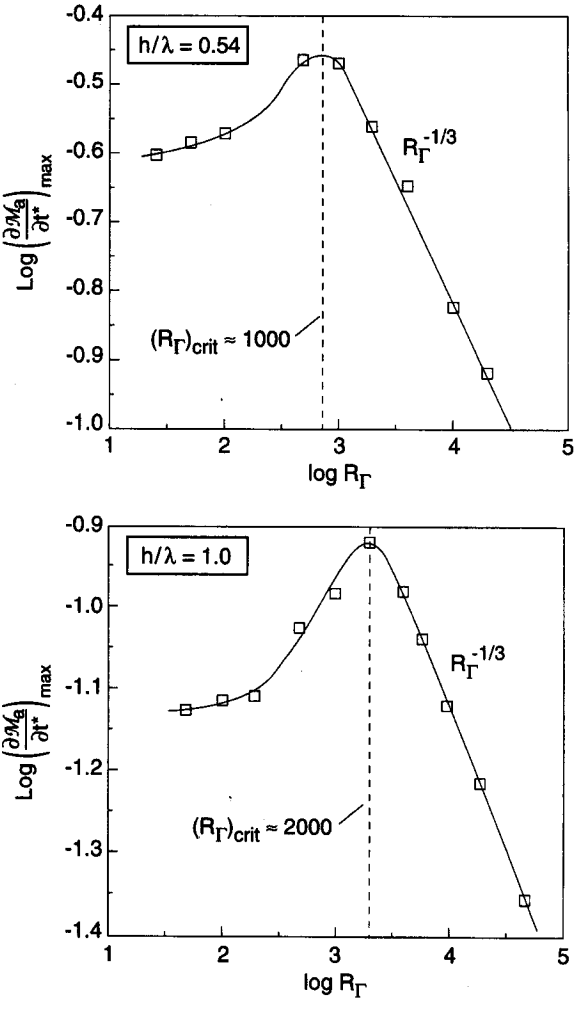

Fig. 11. Maximum scalar mixing augmentation rate as a function of Reynolds number: $Sc = 1.0$.[21]

between either side of the lobed mixer. For these cases, we define the momentum mixing parameter

$$\mathcal{M}_p = \frac{1}{A}\int_A \left(1 - \left(\frac{u'}{\frac{\Delta U}{2}}\right)^2\right) dA \tag{36}$$

as the measure of mixedness and again focus on the augmentation in mixing due to the vortex, $\mathcal{M}_{pa}$ (i.e. that portion of the mixing which is in excess of what would occur for the same trailing edge geometry but with no streamwise vorticity). The computations were carried out for $Sc_t = 1.0$ so that the evolution of the perturbation in axial velocity, u', can be directly related to the evolution of the passive scalar field. The results for the turbulent cases are similar to the laminar results, and two examples are shown in Fig. 12. In Fig. 12a it is seen that the scaling of Equation (34), this time based on the turbulent diffusion coefficient, is applicable for velocity ratios of 0.67 and 0.8 for $t^* \leq 1.2$. However, for the cases with larger velocity differences shown in Fig. 12b ($\tau = 0.125$ and $\tau = 0.25$), the scaling represents the behavior of the flow only for $t^* \leq 0.6$.

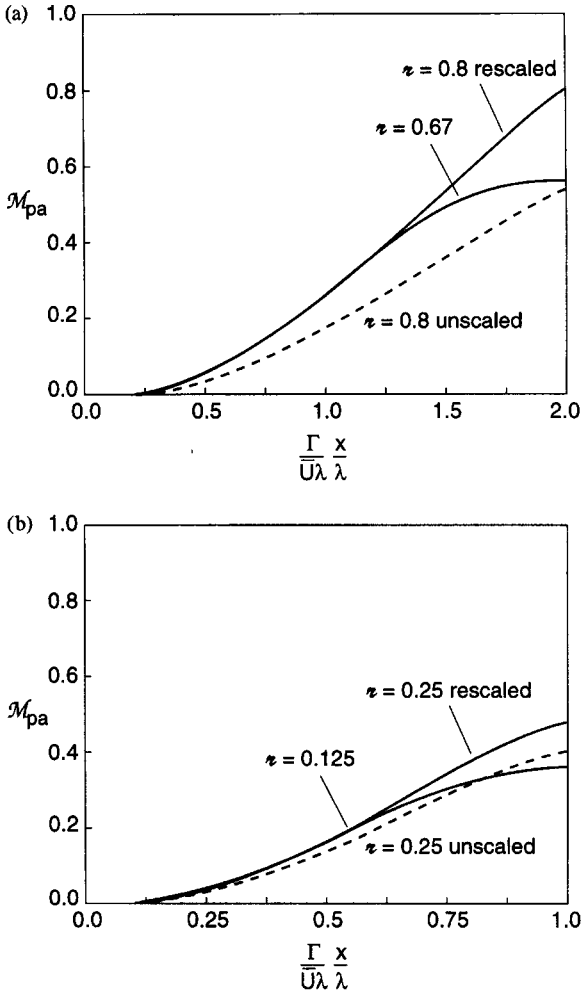

Fig. 12. (a) Momentum mixing augmentation for $h/\lambda = 0.54$ and $\Gamma/\bar{U}\lambda = 0.30$.[21]; (b) momentum mixing augmentation for $h/\lambda = 0.54$ and $\Gamma/\bar{U}\lambda = 0.39$.[21]

5.3. EXPERIMENTAL ASSESSMENT OF THE EFFECT OF STREAMWISE VORTICITY ON MIXING

5.3.1. *Conceptual Basis of the Experiments*

Experiments have been carried out to assess the relative contribution of initial interface length and streamwise vorticity on the mixing downstream of lobed mixers. Two separate sets of experiments were conducted, one which addressed mixing on a molecular scale, such as would be needed for combustion, and one which addressed momentum interchange. The experiments also provide evaluation of the approximations made in the flow description based on the vortex diffusion flame model and the slender body approach.

The central idea is that the effects of initial trailing edge length and the streamwise vorticity can be separated through examination of the flow field associated with the two geometries shown schematically in Fig. 13. These are a lobed mixer, and a lobe configuration, referred to as the convoluted plate, which has the same trailing edge geometry but a parallel extension of the trailing edge. The length of the extension controls the amount of net streamwise vorticity in the flow and so can be used as a diagnostic for understanding the role of the vorticity in mixing enhancement. The convoluted plate shown in Fig. 13 has an extension of length 1.6 times the lobe height, the same initial interface length as the lobed mixer, but a shed streamwise circulation almost an order of magnitude lower. This is demonstrated in Fig. 13, which shows the computed streamwise circulation, obtained from a three-dimensional, Reynolds-averaged, Navier–Stokes computation[11] as a function of distance for the lobed mixer and for the convoluted plate. For the lobed mixer, the circulation increases roughly linearly over the surface of the lobe. This increase is also seen initially with the convoluted plate but then, as the flow turns back to the x-direction in the parallel section, the circulation decreases rapidly. The generation of streamwise circulation is a consequence of the non-uniform aerodynamic loading (in y) on the lobes and hence net

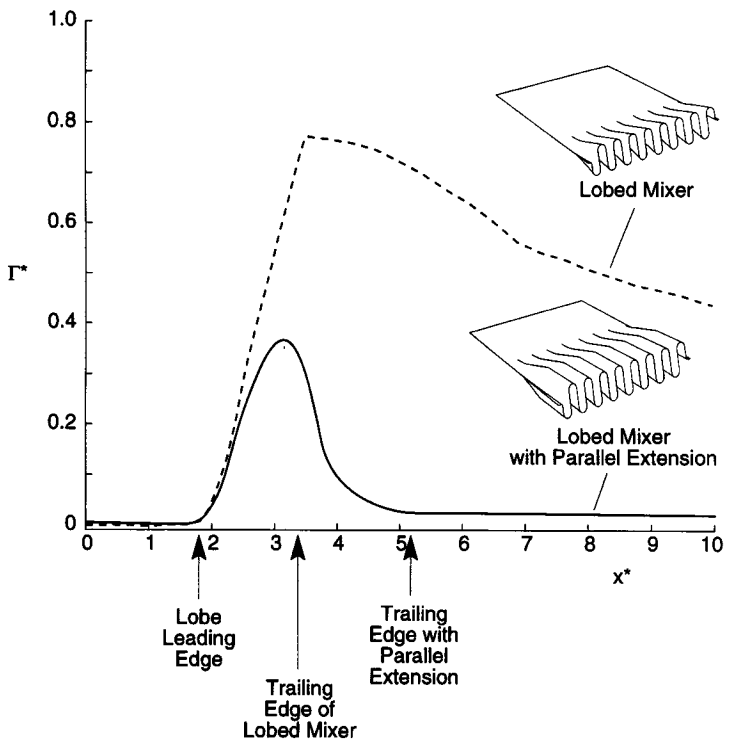

Fig. 13. Streamwise circulation as a function of axial distance for lobed mixer ($\alpha = 22°$, $\iota = 0.6$) and convoluted plate ($\alpha = 22°$, $\iota = 0.53$).[11]

transverse vorticity. This implies a net streamwise circulation, similar to the situation with a finite wing. The parallel extension decreases the non-uniformity in transverse vorticity and hence also the streamwise circulation.

5.3.2. *Water Tunnel Experiments on Molecular Mixing*

Water tunnel experiments to measure molecular mixing have been conducted for the two geometries depicted in Fig. 13, as well as for a conventional flat plate splitter to provide a reference. The experiments were conducted in the facility described in Section 3 and were based on optical measurements of the chemical reaction between the two streams, following the technique used by Breidenthal.[4] In this technique, one stream contains phenolphthalein, the other sodium hydroxide, so that the two streams are initially clear. When mixing at the molecular level has brought the local pH to a level between 8 and 12 the product turns a vivid red. Light directed across the mixing layer is attenuated by the product of the mixing. The degree of attenuation gives a direct measure of the molecular scale mixing. Further details of the facility and the experimental procedure are given by Manning.[12]

Figure 14 shows measured molecular mixedness as a function of axial distance downstream of the trailing edge for the lobed mixer, convoluted plate, and flat plate. Cases are shown where the velocity ratios are $s = 1.0, 0.67, 0.5$. We consider first the convoluted plate to assess the increase in mixing due to increased trailing edge length. In the region in which the shear layers from adjacent lobes have not yet merged (in this experiment for $x/\lambda < 5$), the increase in mixing rate compared to the flat plate is essentially only due to the increase in interfacial surface area at the trailing edge. The convoluted plate trailing edge length was 2.6 times longer than that of the flat plate. For the cases shown with $s = 1.0$ and $s = 0.67$, the ratio of the mixing rates for the convoluted plate and the flat plate fall close to the ratio of the trailing edge lengths*.

The mixer lobe introduces streamwise vorticity and hence additional mixing. In this case, the additional mixing due to the streamwise vorticity is roughly the same amount as that due to the increased trailing edge length. The experiments demonstrate clearly, however, the roles of both the increase in initial interfacial surface area and the further stretching of the interface due to the streamwise vorticity in mixing augmentation.

We can also compare the scaling for mixing augmentation expressed in Equation (31) with the measurements. The augmentation in mixing rate is the difference between the slopes of the mixing curves for the lobed mixer and the convoluted plate. From Fig. 14, the curves are roughly linear between $2 \lesssim x/\lambda \lesssim 4$. In this region, the ratio between the mixing augmentation rates for $s_2 = 0.67$, and $s_3 = 0.5$, is $(\mathrm{d}\mathcal{M}_a/\mathrm{d}x)_2/(\mathrm{d}\mathcal{M}_a/\mathrm{d}x)_3 \approx 0.65$.[12] The ratio of mixing augmentation calculated using Equation (31) with the variation in D_t found using Equation (26) is $(\mathrm{d}\mathcal{M}_a/\mathrm{d}x)_2/(\mathrm{d}\mathcal{M}_a/\mathrm{d}x)_3 = 0.7$, in good agreement with the experimental value.

5.3.3. *Wind Tunnel Measurements of Momentum Mixing*

Measurements of momentum interchange between two streams have also been carried out for the lobed mixer, convoluted plate and flat plate in a low speed wind tunnel (velocities of the order of 40 m s^{-1}). The lobed mixer had a penetration angle of 20 degrees and a height to wavelength ratio of 2.0. The test section was 100×290 mm and 1 m long. The stream-to-stream velocity ratio was set by adjusting the blockage of far upstream perforated plates in the two streams. The Reynolds numbers were roughly 10^5, based on mean velocity and lobe wavelength and 1.4×10^5 based on circulation for the mixer lobe (R_Γ). Further details of the facility are given by Qiu.[21]

* For $s = 0.5$, the flat plate mixing rate shown was obtained using an empirical scaling law since the data that was collected for the flat plate at this condition was in error.[12]

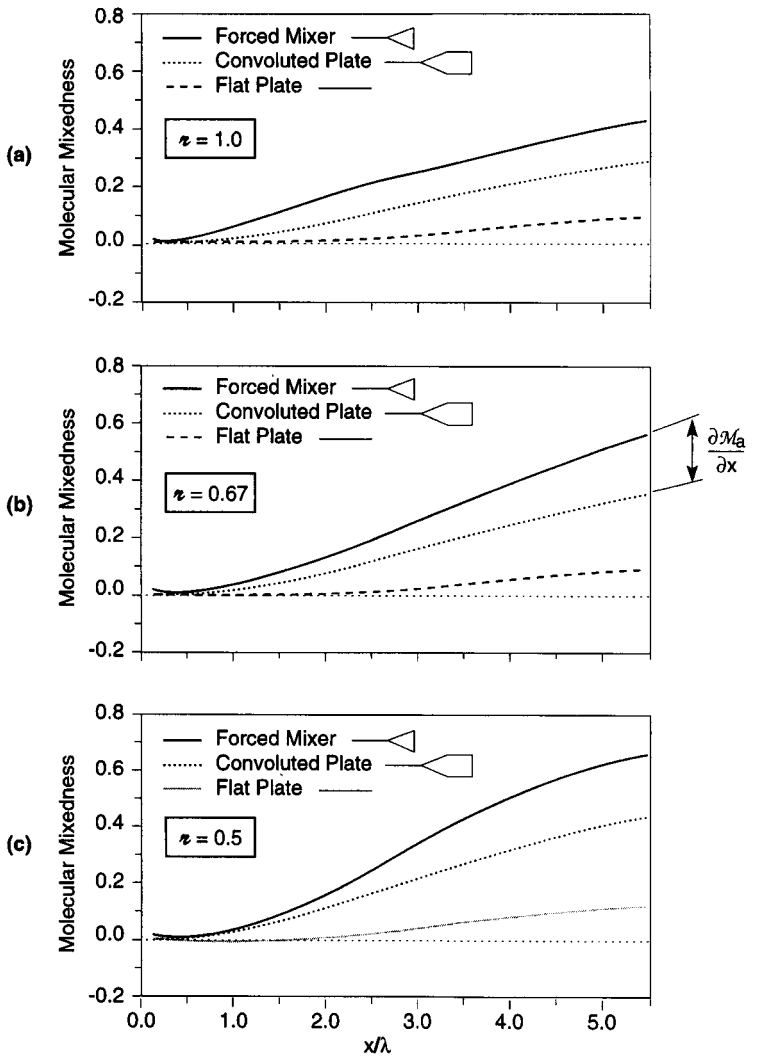

Fig. 14. Mixedness profiles for lobed mixer, convoluted plate and flat plate at velocity ratios; (a) $r = 1.0$; (b) $r = 0.67$; and (c) $r = 0.5$.[12]

The test section was designed with constant area so that the rise in static pressure was directly related to the change in overall momentum flux of the two streams. Measurements of the pressure rise can thus be used to assess the momentum interchange between streams.

Figure 15 shows data for the three configurations: lobed mixer, convoluted plate and flat plate, at a velocity ratio of 0.31. The horizontal axis is the distance downstream from the lobed mixer and the vertical axis is the static pressure rise normalized to the static pressure rise obtained from ideal constant area mixing of two streams each having uniform profiles. The reference pressure is atmospheric pressure (pressure at the mixing duct exit), so the curves represent the extent to which the pressure at the mixer trailing edge is depressed below atmospheric. The pressure rise given has been adjusted for the decrease in static pressure along the duct due to wall friction using results from runs at a velocity ratio of unity (no mixing). Conditions for the lobed mixer and the convoluted plate can be regarded as nearly fully mixed in the test section but the flat plate data cannot. The difference in mixing performance between the lobed mixer and the convoluted plate, i.e. the impact of streamwise vorticity, is evident.

One way to quantify data such as this is in terms of the length that it takes the mixing to occur. For this we can define an integral pressure recovery length as

$$L = \frac{\int \Delta\bar{P}\, \mathrm{d}\,\frac{x}{\lambda}}{(\Delta\bar{P})_{\mathrm{t.e.}}} \tag{37}$$

where $\Delta\bar{P}$ is the average pressure difference between the trailing edge and the mixing duct exit. The integral recovery length which is a measure of how rapidly mixing occurs, is shown as a function of velocity ratio in Fig. 16. Note that the data for a velocity ratio of 0.55 is less

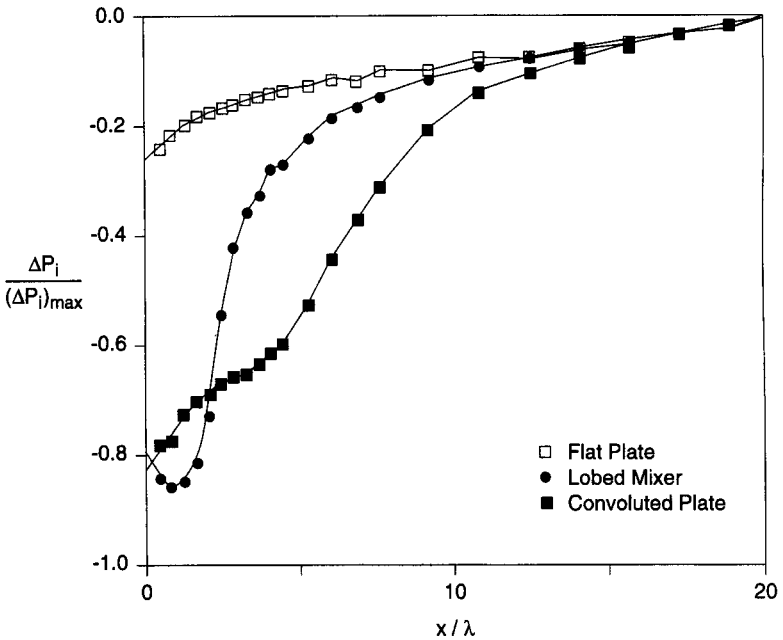

Fig. 15. Comparison of normalized static pressure recovery downstream of the lobed mixer, convoluted plate, and flat plate for velocity ratio of 0.31.[21]

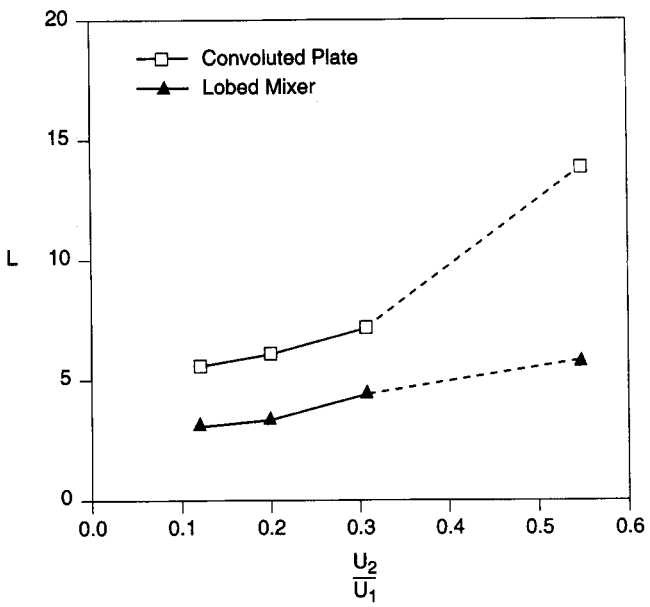

Fig. 16. Comparison of integral length of ideal static pressure recovery as a function of velocity ratio.[21]

reliable because the pressure rise due to the mixing at this velocity ratio is small and the measurement is relatively less accurate. Figure 16 shows that the lobed mixer roughly halves the distance to mix out compared to the convoluted plate.

6. EFFECTS OF COMPRESSIBILITY

The final aspect we discuss concerns the extension of some of the ideas presented to compressible flow. There are two issues to be addressed: (1) the influence of compressibility on the distribution of shed circulation in the downstream region; and (2) the effect on shear layer mixing, or, within the context of the model, the dependence of the diffusivity on Mach number.

For typical mixer nozzle geometries, cross-stream Mach numbers are subsonic for axial Mach numbers of 2 or less. Trends concerning the magnitude and evolution of the streamwise circulation are thus largely unchanged from those at low speed. This is demonstrated in Fig. 7 which shows computational results for average freestream Mach numbers of 0.5 and 2.0.[8] The growth of the time-mean mixing interface in the cross-flow plane, which represents the effect of the vortical structure, is virtually identical for the two Mach number conditions.

Although there is little effect on streamwise circulation, the shear layer mixing is strongly Mach number dependent. The decrease in mixing rate for a planar shear layer due to compressibility is well-documented and has been shown to depend on the convective Mach number, M_c, defined as the relative Mach number of the large-scale structures in the mixing layer with respect to either the low speed or high speed freestream.[18] For $M_c \gtrsim 0.3$ the planar mixing rate begins to be reduced significantly from the incompressible case.[18] If the arguments in Section 4 apply, the decay in vortex mixing with compressibility should scale with the decay in diffusion coefficient to the one-third power and thus with the decay in growth of the planar shear layer vorticity thickness (Equation (25)) to the two-thirds power.

Data on this point is sparse, but there have been back-to-back comparisons of the same mixer lobe with subsonic and supersonic flow. Figure 17 shows data on the temperature non-uniformity along the center-line of a lobed mixer/ejector configuration. With the same velocity ratio of 4:1, measurements were made at two different primary stream Mach

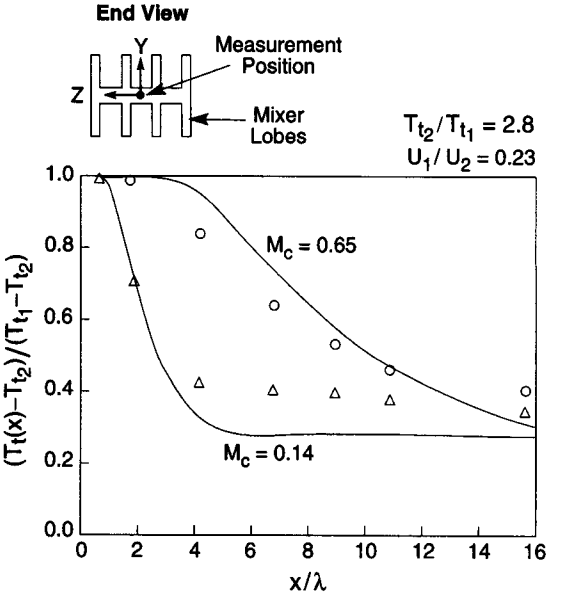

Fig. 17. Computational/experimental comparison for mixing of a temperature nonuniformity with increasing compressibility.[27] M_c is the convective Mach number.

numbers, 0.5 and 1.5 (corresponding to convective Mach numbers of 0.14 and 0.65, respectively).[27] The results of slender body calculations[21] employing an effective diffusion coefficient which has been adjusted to account for the decrease in shear layer growth rate with compressibility are also shown. It is seen that the general trend for less mixing with increasing compressibility is captured by this simplified approach.

7. SUMMARY AND CONCLUSIONS

(1) An experimental and numerical investigation has been conducted of mixing augmentation due to streamwise vortices downstream of forced mixer lobes. The investigation included quantitative descriptions of the principal fluid dynamic processes by which such augmentation occurs and assessment of analytical tools developed to describe these processes.
(2) The role of streamwise vorticity in mixing augmentation has been described quantitatively. Augmentation is due to the strain rate field associated with the vortices, which increases both interface area (the area available for mixing between two streams) and local gradients in fluid properties (the driving potential for mixing across this interface).
(3) An enabling factor in modeling the flows of interest is that for many practical devices the scale of the motions associated with the transverse vorticity is initially much less than the scale of the cross-stream convective transport associated with streamwise vorticity. This difference in scale allows application of a slender body analytical framework in which the 3-D steady flow is usefully viewed as a 2-D unsteady flow in a coordinate system traveling with the mean reference velocity.
(4) First of a kind experiments have been carried out to quantify: (1) the increase in mixing associated with the streamwise vortices shed from the lobed mixer; and (2) the increase in mixing due to the increased trailing edge length of the lobes. For the class of lobes examined, which are representative of current mixer configurations, the two effects were found to be of roughly equal magnitude.
(5) The experiments carried out on both bulk momentum mixing and molecular scale mixing show that the models and scaling laws presented give useful descriptions of the effects of lobe geometry, Reynolds number, stream-to-stream velocity ratio, and mean Mach number, on overall mixing and flow field structure.

ACKNOWLEDGEMENTS

The research and ideas of many people influenced the work discussed in this paper. In particular we wish to thank Dr D. C. McCormick for elucidating several important aspects of these flows and for providing many insightful comments about the work. We also thank Professor N. A. Cumpsty for very helpful suggestions and critical review of the manuscript at several stages. Professor W. N. Dawes, Professor J. Peraire, Dr W. M. Presz Jr and Dr T. J. Barber provided much help and guidance over the last several years which we are also pleased to acknowledge. We are grateful for the support provided by NASA Lewis Research Center through Grant NAG3-1364 with technical monitor Mr James R. DeBonis, by NASA Langley Research Center through Grant NAG-1-1511 with technical monitor Dr John M. Seiner and by the Naval Air Systems Command via Contract #N00019-88-C-0229 and program managers Dr L. Sloter and Mr G. Derderian. We also offer our sincere thanks to Diana Park for her expert help and advice on preparing the text and graphics for this manuscript.

REFERENCES

1. Anderson, B. H., Povinelli, L. A. and Gerstenmaier, W. (1980) Influence of pressure driven secondary flows on the behavior of turbofan forced mixer nozzles, AIAA Paper AIAA-80–1198.

2. Barber, T. J., Paterson, R. W. and Skebe, S. A. (1988) Turbofan forced mixer lobe flow modeling, I—Experimental and analytical assessment, II—three-dimensional inviscid mixer analysis (FLOMIX), III—application to augmentor engines. NASA CR 4147.
3. Batchelor, G. K. (1967) *An Introduction to Fluid Mechanics*, Cambridge University Press, Cambridge, U.K.
4. Breidenthal, R. E. Jr (1979) A chemically reacting turbulent shear layer, Ph.D. Thesis, California Institute of Technology, Pasadena, CA.
5. Brown, G. L. and Roshko, A. (1974) On density effects and large structure in turbulent mixing layers, *J. Fluid Mech.* **64**, 775–816.
6. Dawes, W. N. (1992) The practical application of solution-adaptation to the numerical simulation of complex turbomachinery problems, *Prog. in Aerospace Sci.*, **29**, 221–269.
7. Dimotakis, P. E. (1991) Turbulent free shear layer mixing and combustion. GALCIT Report FM91-2, California Institute of Technology. [See also Dimotakis, P. E. (1989) Turbulent free shear layer mixing and combustion. AIAA paper 89-0262, 27th Aerospace Sciences Meeting.]
8. Elliot, J. K. (1990) A computational investigation of the fluid dynamics of a three-dimensional, compressible, mixing layer with strong streamwise vorticity, S.M. Thesis, Department of Aeronautics and Astronautics, Massachusetts Institute of Technology, MA.
9. Fung, A. K. S. (1995) Modeling of mixer-ejector nozzle flows, S.M. Thesis, Department of Aeronautics, and Astronautics, Massachusetts Institute of Technology, MA.
10. Karagozian, A. R. and Marble, F. E. (1986) Study of a diffusion flame in a stretched vortex, *Combustion Sci. Technol.* **45**, 65–84.
11. Kransnodebski, J. K. (1995) Numerical investigations of lobed mixer flow fields, S.M. Thesis, Department of Mechanical Engineering, Massachusetts Institute of Technology, MA.
12. Manning, T. A. (1991) Experimental studies of mixing flows with streamwise vorticity, M.S. Thesis, Massachusetts Institute of Technology, Cambridge, MA.
13. Marble, F. E. (1987) Chemical reactivity in liquids. In: *Proc. 4nd Int. Meeting*, Division de Chimie Physique, Societe Francaise Chimie, Paris.
14. Marble, F. E. (1985) Growth of a diffusion flame in the field of a vortex, *Recent Advances in the Aerospace Sciences*, Plenum Publishing, New York.
15. Marble, F. E., Zukoski, E. E., Jacobs, J. W., Hendricks, G. J. and Waitz, I. A. (1990) Shock enhancement and control of hypersonic mixing and combustion, AIAA Paper 90-1981.
16. McCormick, D. C. (1992) Vortical and turbulent structure of planar and lobed mixer free-shear flows, Ph.D. Thesis, University of Connecticut, CT.
17. O'Sullivan, M. N., Waitz, I. A., Greitzer, E. M., Tan, C. S. and Dawes, W. N. (1996) A computational study of viscous effects on lobed mixer flow features and performance. *AIAA J. Propulsion and Power.*
18. Papamoschou, D. and Roshko, A. (1988) The compressible turbulent shear layer: an experimental study, *J. Fluid Mech.* **197**, 453–477.
19. Peiro, J., Peraire, J. and Morgan, K. (1993) Felisa system reference manual, Part I—Basic theory.
20. Presz, W., Gousy, R. and Morin, B. (1986) Forced mixer lobes in ejector designs AIAA Paper AIAA-86–1614, *22nd Joint Propulsion Conference.*
21. Qiu, Y. J. (1992) A study of streamwise vortex enhanced mixing in lobed mixer devices, Ph.D. Thesis, Massachusetts Institute of Technology, Cambridge, MA.
22. Schlichting, H. (1979) *Boundary Layer Theory*, 7th edn, McGraw-Hill Inc., New York, NY.
23. Skebe, S. A., McCormick, D. C. and Presz, W. M. (1988) Parameter effects on mixer–ejector pumping performance, AIAA Paper AIAA-88-0188, *26th Aerospace Sciences Meeting.*
24. Skebe, S. A., Paterson, R. W. and Barber, T. J. (1988) Experimental investigation of three-dimensional forced mixer lobe flow fields, AIAA Paper AIAA 88-3785.
25. Tan, C. S. (1985) Accurate solution of three-dimensional Poisson's equation in cylindrical coordinates by expansion in chebyshev polynomials, *J. Comp. Phys.* **59**, 81–95.
26. Tew, D. E. (1992) A computational study of mixing downstream of a lobed mixer with a velocity difference between the co-flowing streams, S.M. Thesis, Department of Aeronautics and Astronautics, Massachusetts Institute of Technology, MA.
27. Tillman, T. G., Paterson, R. W. and Presz, W. M. (1992) Supersonic nozzle mixer ejector, *J. Propulsion Power* **8**, 513–519.

APPENDIX A

APPLICABILITY OF THE SLENDER BODY APPROACH

In the derivation of the slender-body system of equations (Equations (17)–(20)) it was stipulated that the axial velocity perturbations satisfy $|u'|\bar{U}| \ll 1$ and that the circulation satisfies $\Gamma/\bar{U}\lambda \ll 1$. Neither of these two requirements is rigorously met in devices of practical interest. For example, from Equation (2)

$$\frac{\Gamma}{\bar{U}\lambda} \approx 2\frac{h}{\lambda}\tan(\alpha). \tag{A.1}$$

If $h/\lambda \sim 1.0$, and $\tan\alpha = 25°$, which are not untypical, then $\Gamma/\bar{U}\lambda \sim 0.9$. Further, for a velocity ratio $r = U_1/U_2 = 0.5$ for example, the axial velocity perturbation is $|u'/\bar{U}| = 0.33$. Thus, neither of these quantities satisfies the formal restrictions. To assess in more detail the degree to which the slender-body approach is applicable, we have carried out comparisons with fully three-dimensional simulations. These not only illustrate important features of these flows, but also show that the slender-body approximation gives useful results over the range of parameters of practical interest.

The three-dimensional simulation of the flow over and downstream of a lobed mixer was carried out using a Reynolds-averaged, Navier–Stokes solver developed by Dawes, which employs a k–ε turbulence model.[6,17] The code has been used extensively for turbomachinery and internal flow calculations and was validated for this application by Krasnodebski.[11] The integration was carried out on an unstructured grid which was generated using an advancing front technique.[19] For the slender-body computations (solution of Equations (17)–(20)) a spectral element Navier–Stokes code was used. The computational domain was divided into 128 elements; within each element the flow field variables were represented with 7×7-order Chebychev polynomials.[21,25] To ensure

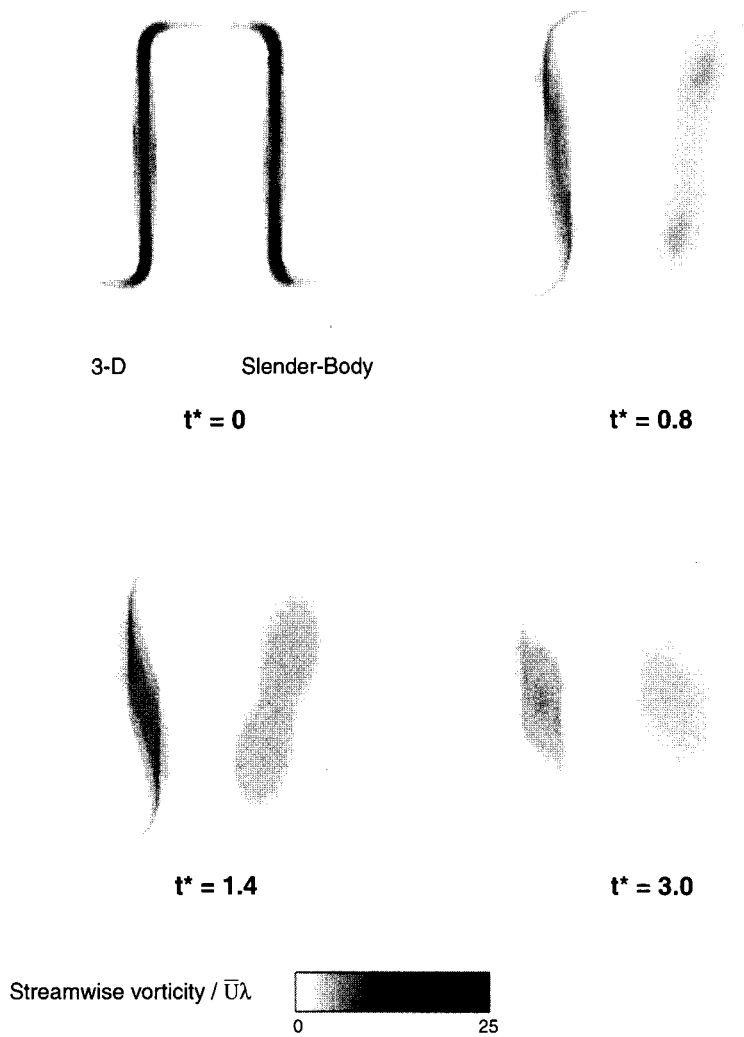

Fig. A.1. Comparison of 3-D and slender-body streamwise vorticity distribution at $t^* = 0$, 0.8, 1.4, 3.0 ($r = 1.0$, $s = 1.0$).

consistent comparison, the slender-body calculations were initiated at the trailing edge using the streamwise vorticity distribution taken directly from the three-dimensional solution. The turbulent viscosity and the scalar diffusion coefficient were also kept the same between the two codes. The lobes had $h/\lambda = 1.0$ and lobe penetration angle, $\alpha = 22°$, for which $\Gamma/\bar{U}\ \lambda = 0.9$. The velocity ratio between the freestreams on either side of the lobed mixer was specified from $\imath = 0.6$ to $\imath = 1.0$. In the simulations a scalar was specified: $\phi = -1$ below the lobed mixer and $\phi = +1$ above the mixer. Two aspects will be addressed: the overall flow features and the mixedness.

We first present the results for $\imath = 1.0$. The evolution of the streamwise vorticity field as captured in the two simulations is compared in Fig. A.1 and the scalar field is shown in Fig. A.2. The time $t^* = 0.0$ is at the lobe trailing edge. The thickness of the region of appreciable vorticity reflects a computed boundary layer thickness at this location. Figure A.1 illustrates the rotation and roll-up of the distributed sheet of vorticity into a discrete

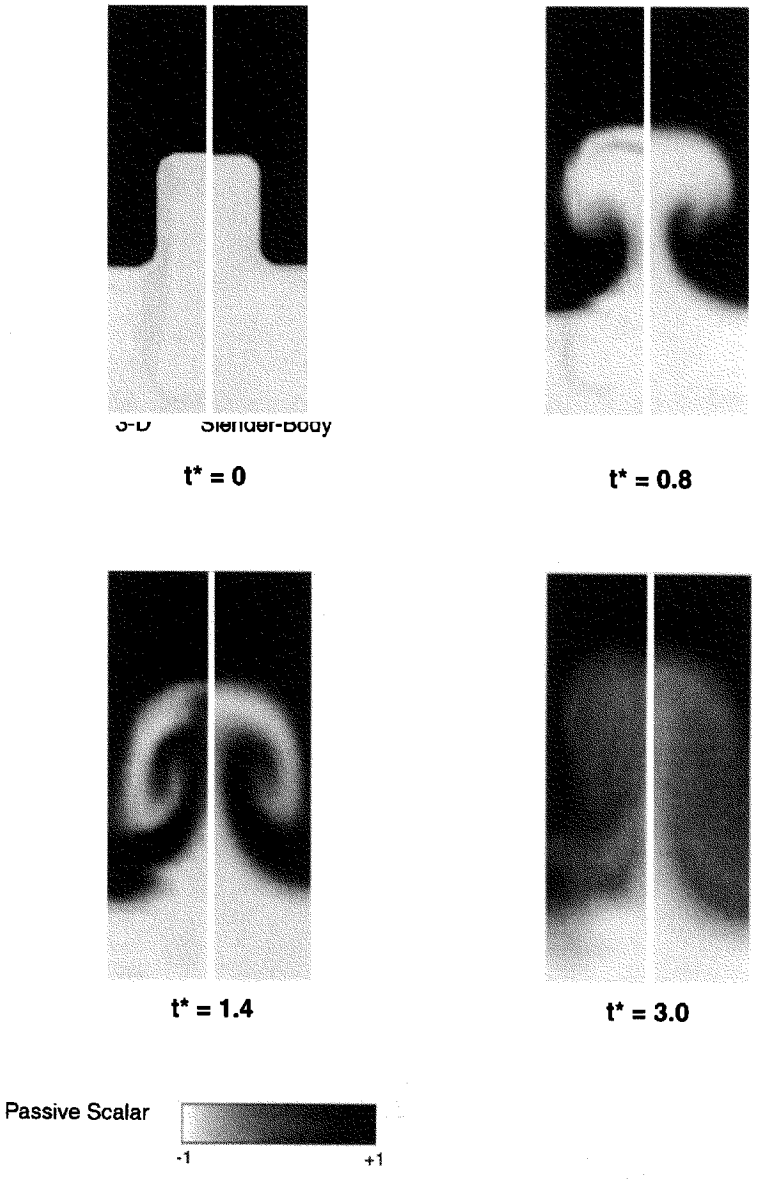

Fig. A.2. Comparison of 3-D and slender-body passive scalar distribution at $t^* = 0, 0.18, 1.4, 3.0$ ($\imath = 1.0$, $s = 1.0$).

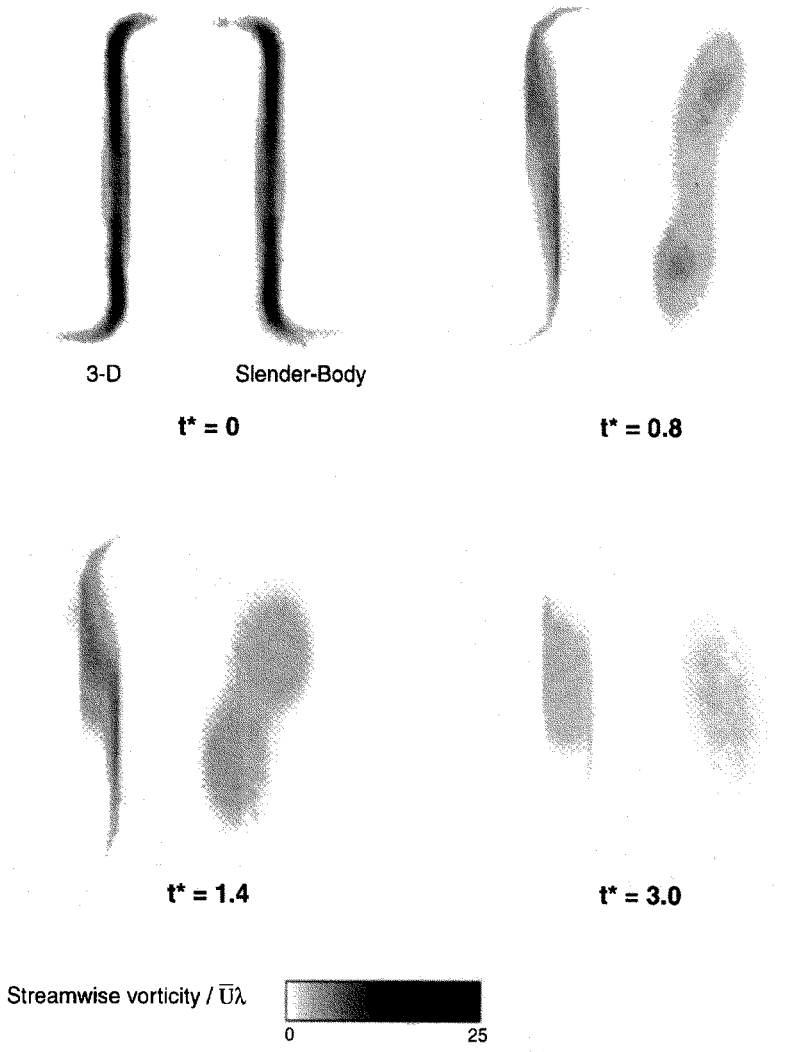

Fig. A.3. Comparison of 3-D and slender-body streamwise vorticity distribution at $t^* = 0$, 0.8, 1.4, 3.0 ($\iota = 0.6$, $s = 1.0$).

core which is eroded by viscous diffusion. The velocity field associated with the vortex has a dramatic effect on the mixing of the scalar property field, as shown in Fig. A.2 which gives contours of the scalar variable at the same times. The effect of the increases in interface length are evident. At $t^* = 3.0$, it can be seen that the interface has been stretched to roughly double its initial length. In Figs A.3 and A.4 we present the results for the case with $\iota = 0.6$ which represents a more severe test of the slender body calculations. Although the overall flow features are similar, the differences between the results of the fully three-dimensional computation and the slender body analysis are more significant for the case of $\iota = 0.6$ than for the case of $\iota = 1.0$.

It is also important to assess the mixing on a quantitative basis, since this is a main item of interest. A comparison of mixedness (defined using Equation (34)) as a function of downstream distance for the slender-body and three-dimensional computations is shown in Fig. A.5 for the cases $\iota = 1.0$ and $\iota = 0.6$. In the region $t^* < 3$ where most of the mixing augmentation occurs, the mixing rate for the slender body code is 10% less than that for the three-dimensional simulation for $\iota = 1.0$. The accuracy of the slender body simulation

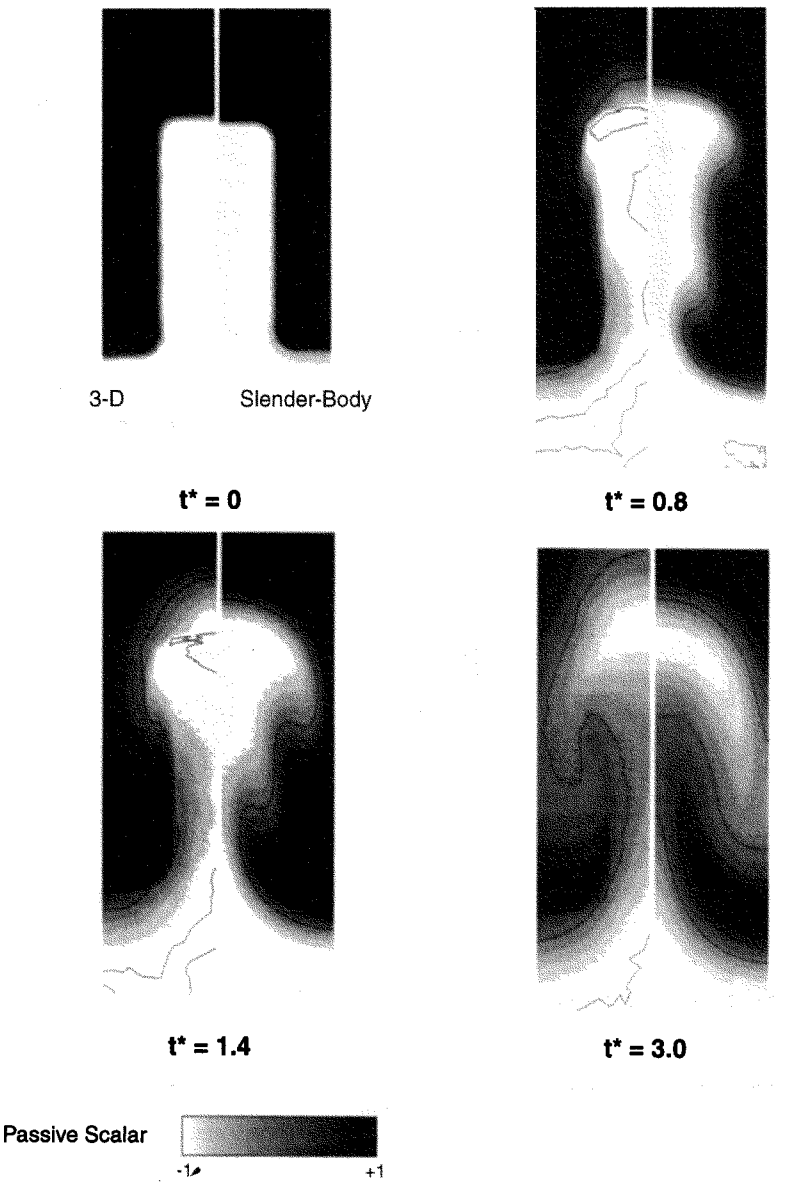

Fig. A.4. Comparison of 3-D and slender-body passive scalar distribution at $t^* = 0, 0.8, 1.4, 3.0$ ($\lambda = 0.6$, $s = 1.0$).

degrades as the velocity difference between the two streams increases. For the case $\lambda = 0.6$ shown in Fig. A.5, the difference in mixing rate between the three-dimensional and the slender body simulations is 25%.

The slender body simulations were also assessed by comparing them to results from the wind tunnel experiments described in Section 5.3.3. Figure A.6 shows a comparison of slender body computations and experiments for a lobed mixer at three different velocity ratios, $\lambda = 0.13$, 0.20 and 0.30. The pressure rise was obtained from the slender-body calculations by assuming that $Sc_t = 1$ and that scalar and axial momentum mixedness have the same behavior. The numerical results compare well with experimental data over the range shown, even though the ratio of axial velocity non-uniformity to mean axial velocity is 0.75 when $\lambda = 0.13$, a rather severe test of the slender body approach.

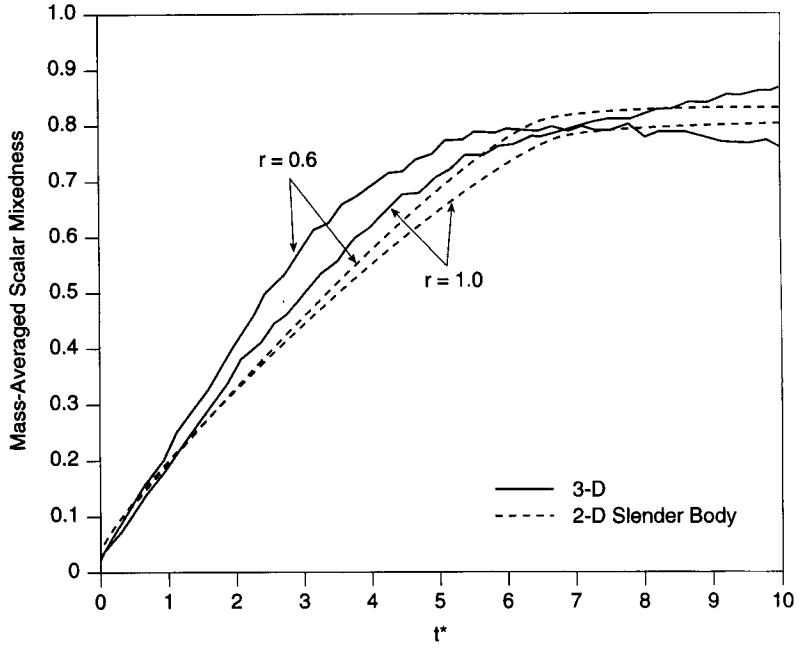

Fig. A.5. Comparison of 3-D and slender-body area-averaged scalar mixedness.

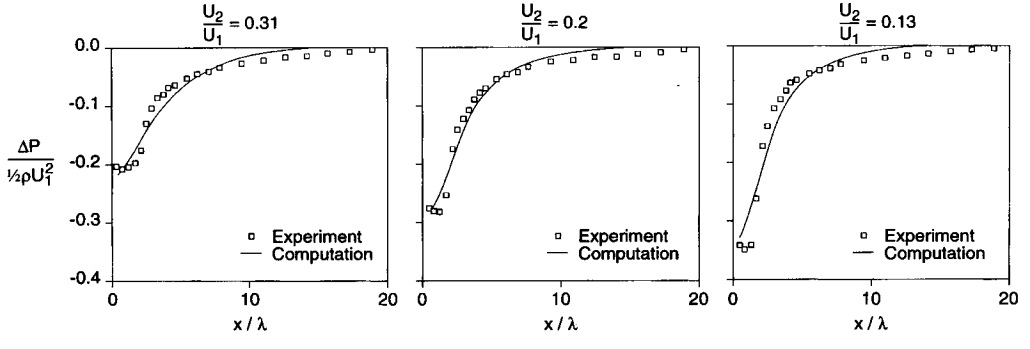

Fig. A.6. Comparison of experimental static pressure recovery downstream of the lobed mixer with computations.[21]

From these comparisons it is apparent that the slender-body flow is a useful approximation to the three-dimensional flow for realistic mixer lobe geometries or, in other words, that the two-dimensional, unsteady scaling laws can be used to describe the three-dimensional flow field downstream of the lobed mixer.